

A comparative analytical study on the fragility assessment of box-girder bridges with various column shapes



Farahnaz Soleimani*, Sujith Mangalathu, Reginald DesRoches

School of Civil and Environmental Engineering, Georgia Institute of Technology, Atlanta, GA 30332, United States

ARTICLE INFO

Keywords:

Fragility analysis
 Probabilistic seismic demand model
 Concrete box-girder bridge
 Seismic response
 Fragility curve
 Column cross-section shape
 Prismatic column
 Flared column
 Oblong column
 Circular column
 Rectangular column

ABSTRACT

Bridge columns are known as the most vulnerable components of a bridge and operate as the core substructure elements of the bridge support system. Post-earthquake evidence reveals that large deformation and extensive damage of bridge columns are linked to the force and deformation capacity of the columns. Since research on the seismic vulnerability of bridges with various column shapes is limited, this paper aims to address this deficiency by evaluating the seismic performance of a variety of common column shapes. This analytical study involves assessing circular, rectangular, and oblong-shaped columns. Each shape of the column is tested as prismatic or flared along the column height as many of the bridges, constructed after 1970 in high seismic zone areas like California, are supported by flared columns. First, the study concentrates on assessment of several different column shapes as individual elements through both monotonic and cyclic pushover analysis. Second, a complete bridge system is investigated for the impact of the cross-section shapes and column flares on the fragility assessment findings. This article deals with the seismic vulnerability assessment of box-girder types bridges. A set of numerical bridge models that accounts for geometric and material uncertainties according to the California bridge characteristics is created in OpenSees. According to the results, oblong columns display less fragility compared to the other column shapes. The comparison of the seismic analysis for prismatic and flared columns shows the vulnerability of flared columns. The findings indicate that neglecting the effect of column shapes on the bridge fragilities leads to an unreliable estimation of the seismic risk and associated losses.

1. Introduction

Bridges are the critical links in a transportation network and their seismic vulnerability can lead to large economic losses. Bridge vulnerability can be assessed by developing fragility curves that indicate probability of reaching or exceeding a specific level of damage. According to the plan review of the existing box-girder bridges in California, the typical configuration of bridge columns consists of circular and rectangular cross-section shapes (Fig. 1) with constant cross-section dimensions along the column height also known as prismatic columns. However, other column configurations exist that can alter the seismic performance of columns and bridges. These configurations include oblong and flared columns. The seismic fragility analysis of many types of highway bridges in the United States has been explored. Although non-prismatic columns or non-typical column cross-section shapes support many bridges in the United States, most existing studies on fragility analysis [1–10] focus on bridges supported by prismatic columns with circular or rectangular cross-sections. In order to determine the effects of various column shapes, the current study attempts

to evaluate the seismic performance of bridges with oblong and flared columns.

Using oblong column shapes in box-girder bridges can considerably reduce the required amount of transverse reinforcement, as the oblong cross-sections include interlocking spirals. These spirals confine the core concrete more effectively than single spiral confinements and rectangular hoops. Additionally, when a cross-section includes overlapping confinements, fabrication is easier for interlocking spirals than for overlapping rectangular hoops. Tanaka and Park [11] tested four column specimens to study the behavior of columns with interlocking spirals; one with a rectangular shape that contained rectangular hoops, and three with oblong cross-sections that contained interlocking spirals. The tests were performed by applying constant axial loads, equal to ten percent of the axial capacity of the column, and cyclic horizontal loads to the tops of the columns. The experiments showed that the oblong-shaped columns outperformed the rectangular columns in the aspects of stable hysteresis loops, greater energy dissipation, and limited strength reduction up to a displacement ductility demand of approximately 10. Wu, et al. [12] investigated the effect of transverse confinements on the

* Corresponding author.

E-mail address: soleimani@gatech.edu (F. Soleimani).

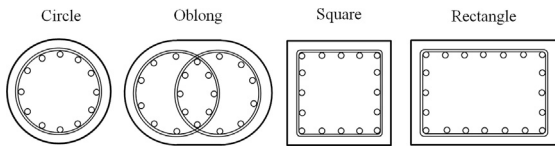


Fig. 1. Cross-section of reinforced concrete columns with various shapes.

performance of oblong and rectangular bridge columns in which either tie or spiral reinforcements were used. Four columns were tested, using combined axial and flexural loadings during the tests. The commonly used column cross-sections are circular and rectangular. A spiral reinforcement scheme is typically advised for circular cross-sections while tied rectangular hoops are typically advised for rectangular cross-sections. In order to take advantage of the benefits of spiral reinforcement, Wu et al. proposed an innovative transverse reinforcement arrangement for rectangular-shaped columns. This arrangement included two central interlocking spiral reinforcements similar to the oblong cross-section. However, four small spirals at the corners of the rectangular cross-section were also added to the section. All of the tested columns displayed satisfactory ductile behavior. Although the two oblong columns exhibited similar behavior, Wu et al. [12] illustrated the improved performance of rectangular columns with spiral reinforcement compared to the tied columns. Ingham et al. [13] conducted a set of experiments at UCSD on large-scale bridge knee-joints, which had a pre-1970 design. The as-built and retrofitted units were tested, and the columns had interlocking spirals. The observed damage during cyclic loading tests of the as-built unit indicated that there were insufficient transverse reinforcements within the joint. However, the retrofitted units with more confinements helped to prevent lap splice failure and inelastic action in the joint. The columns had interlocking spirals. Ou et al. [14] focused solely on the shear behavior of oblong columns, with several different transverse reinforcement schemes, including the conventionally-tied, two-spiral interlocking, and seven-spiral interlocking reinforcements. They proposed the seven-spiral configuration since the large size of the two-spiral oblong columns often poses challenges for fabrication and transportation. The tested columns with their proposed seven-spiral configuration effectively addressed the size issue and showed better performance with greater effective shear coefficients compared to the conventionally-tied columns, while remaining interlocked during the entire experiment.

In addition to typical columns, which have a prismatic configuration, flare-shaped columns with one-way and two-way flares (Fig. 2) also exist. Besides the architectural inclination, one-way flared columns are commonly used in post-1970 bridges to provide more support to the cap beam under eccentric live loads. Flared columns are constructed in

two different ways by either integrating them to the superstructure (these are called connected flares), or by connecting them to the superstructure with a gap in between (these are called isolated flares). The latter type is typically seen in bridges designed after 1990. Sanchez et al. [16] conducted experimental studies on flared columns and concluded that the seismic performance of isolated flares is similar to prismatic columns. This paper is limited to connected, one-way flared columns.

Nada et al. [17] conducted an experimental and numerical study on four flared specimens in which two specimens were designed to display flexural dominant behavior, while the remaining two shorter columns were designed to exhibit shear dominant behavior. Each of the two column types contained different transverse reinforcement designs. One was designed to have consistent confinement along the column height, and the other was designed to contain higher confinements at the top third of the column height. The columns were subjected to eleven ground motions simulated by a shake table. The study showed satisfactory ductile behavior for all tested specimens. Nada et al. [17] strongly recommended including a gap between the short columns and the superstructures since their analysis showed premature failure caused by brittle shear damage. In the case of isolated columns, extensive shear cracks were observed since the gap was closed at a low ductility ratio. As a consequence, the load carrying capacity was increased which caused higher load transferring to the columns. Wehbe et al. [18] examined four half-scaled flared bridge columns. The specimen designs were according to the 46th and 60th percentages of minimum confinements required by AASHTO. The columns were subjected to quasi-static cyclic lateral loadings. Two different longitudinal reinforcement arrangements were used in the tests. In one arrangement, reinforcements were placed along the flares, while in the other, reinforcements were located mainly in the core area. Test results showed higher vulnerability for the flared columns with longitudinal reinforcements distributed along the flares and not concentrated in the core area.

While a number of researchers have studied the seismic performance of bridge columns with various shapes, the effect of column shapes (cross-section and flares) on the fragility assessment of bridge columns and systems is not yet well-known. The current study attempts to address this research gap by evaluating the seismic performance of a typical bridge column as an individual element and as a component of a bridge system. This numerical study is divided into two stages where the structural characteristics of existing box-girder bridges located in California are used as a case study to generate finite element models. First, three-dimensional numerical models of a typical bridge column were created in OpenSees; the models include columns with various common shapes including circular, rectangular, and oblong cross-

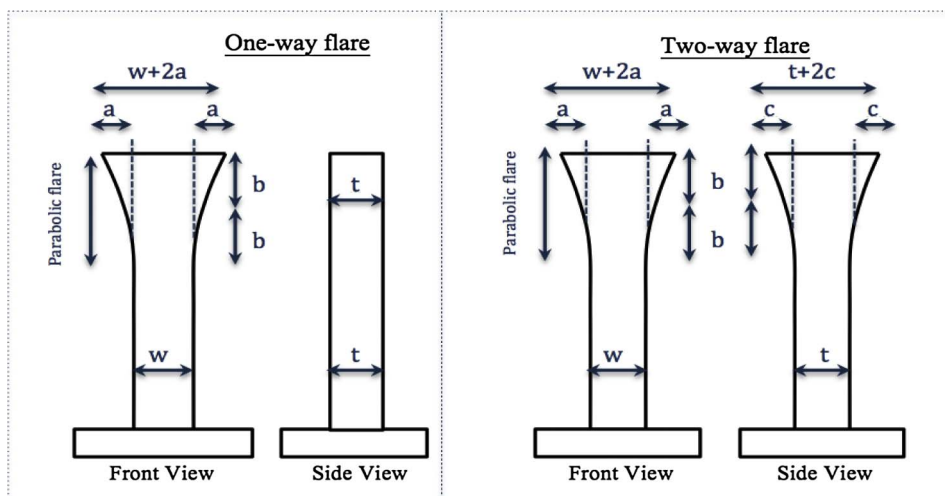


Fig. 2. One-way and two-way flared columns according to the Caltrans Seismic Design Code [15].

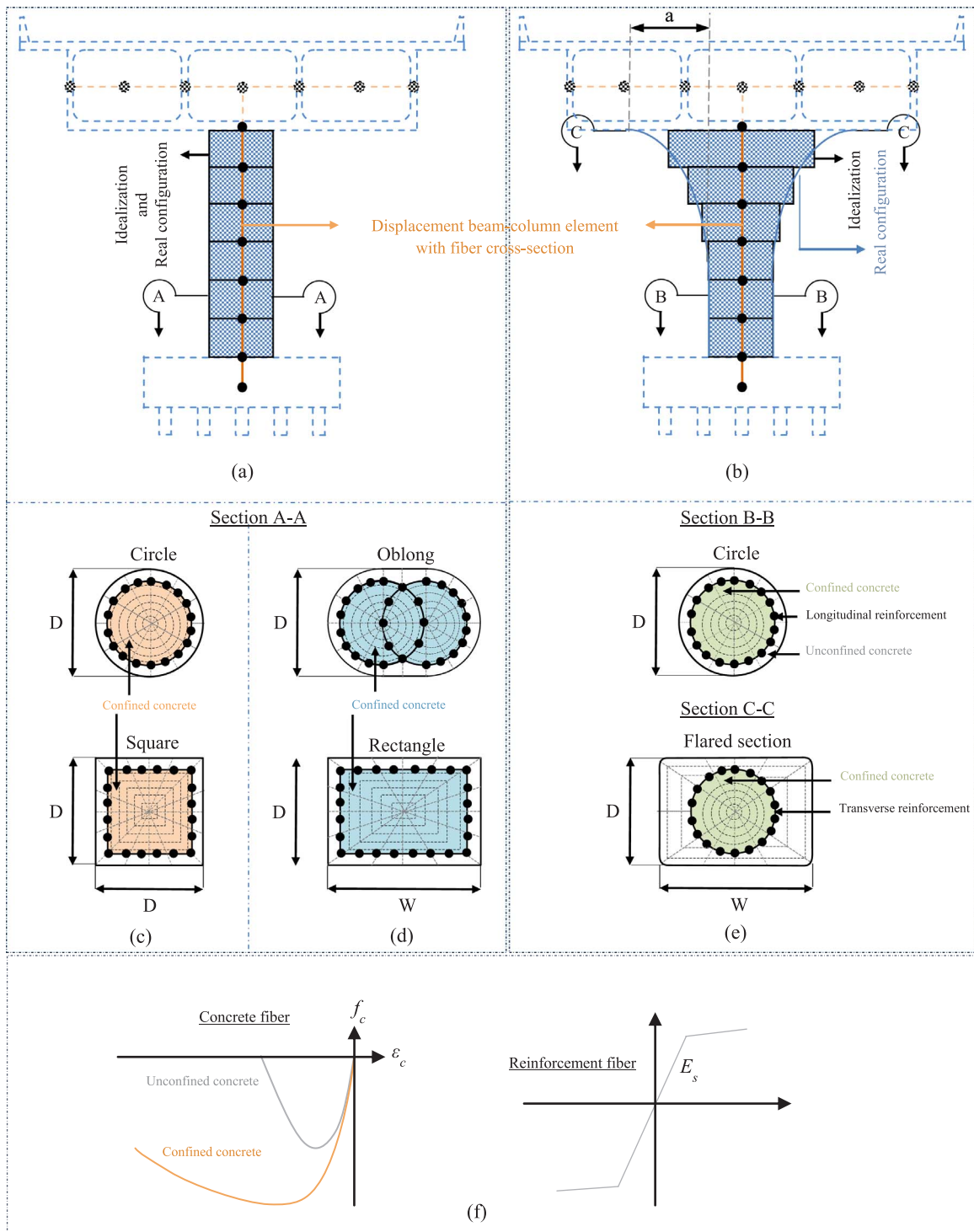


Fig. 3. Column configurations in box-girder bridges for: (a) Prismatic columns, (b) Flared columns, (c) Type I cross-section shapes, (d) Type II cross-section shapes, (e) Type III cross-section shapes, (f) OpenSees material objects assigned to the fiber cross-section.

sections, as well as prismatic and flared columns. The numerical models were validated with previous experiments performed on the column shapes that are considered in this study (Section 2). Then, seismic assessment of typical bridge columns was conducted through a set of monotonic and cyclic pushover analysis (Section 3). Second, a three-dimensional numerical model of a typical box-girder bridge was developed using a variety of column shapes. Using a selected set of ground motions, nonlinear time history analysis was performed on the models to derive structural responses. Next, the seismic performance of the bridge models was evaluated by comparing their probabilistic seismic

demands, particularly the column displacement ductility demand (Section 4). Since developing probabilistic seismic demand models is an essential step toward generating fragility curves, the comparison of the seismic demands provides initial insight into the influence of column shape on the fragility assessment of bridge components. The evaluation process was then continued to produce fragility curves for the various bridge components and the bridge system (Section 4). Assessment of the generated curves indicates the impact of column shapes on the bridge fragility assessment.

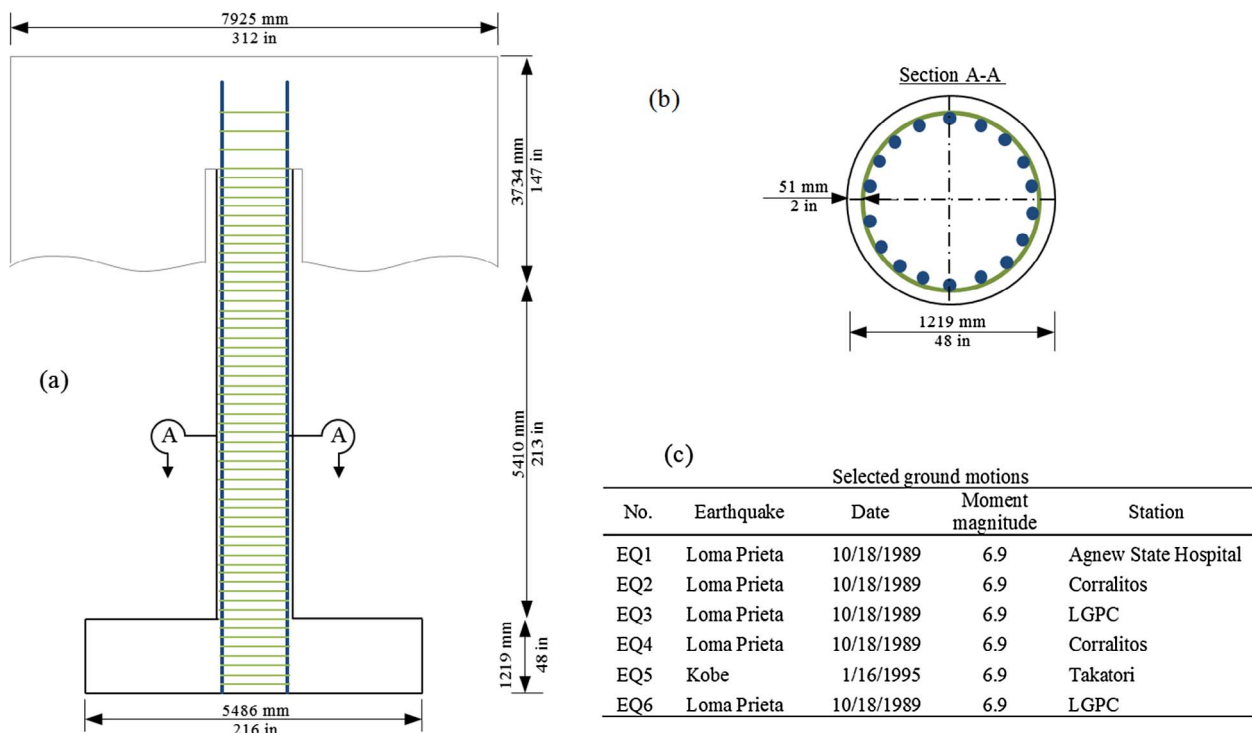


Fig. 4. (a) Details of the UCSD column design, (b) Reinforcement detailing of the UCSD column, (c) selected ground motions.

2. Modeling of bridge columns

2.1. Numerical model

This case study focuses on the most common standardized column shapes in California box-girder bridges. According to the existing bridge configurations, column shapes are categorized into three main categories with layouts shown in Fig. 3: Types I and II fall under the category of prismatic columns (Fig. 3a), while Type III is representative of flared columns where stepped discretization (Fig. 3b) is used to create their numerical models. Type I columns are defined as circular or square-shaped cross-sections in which two adjacent sides have equal lengths, while Type II columns are oblong or rectangularly-shaped, with unequal adjacent sides in the cross-sections.

Displacement-based beam-column elements with fiber-defined cross-sections were used in OpenSees [19,20] to create three-dimensional models of a bridge column (Fig. 3). Fiber elements have a distinct advantage of assigning unique material properties to different locations across a member's cross-section. Concrete 07 and Steel 02 materials in OpenSees were used to model concrete and reinforcing steel, respectively. The Chang and Mander [21] model was used to define the monotonic stress-strain curves of confined and unconfined concrete. The Menegotto and Pinto [22] model, later modified by Filippou et al. [23], was used to add isotropic strain hardening for the reinforcing steel. The bond-slip is not modeled in the current study as the splicing of the longitudinal reinforcement with starter bars extending from the footing is not a common design feature of bridges constructed after 1970. Note that the strain penetration effect is not modeled in the current study as the cyclic force-displacement response is not significantly affected by the strain penetration effect for the selected bridge columns [24]. A more comprehensive description of the numerical modeling of bridge columns can be found in the work of Soleimani [25].

2.2. Verification of numerical model

One initial step in an analytical study is to test the efficacy of

modeling assumptions. In order to validate the model with the aforementioned column shapes, three-dimensional finite element models of the specimens were generated in OpenSees and compared to four column tests selected from previous experiments. The experiments include shake table tests at UC San Diego [26] and cyclic pushover tests by Tanaka and Park [11], and Sanchez et al. [16]. Based on a comparison of the numerical results and experiments data, insights are provided on each of the specimens. A detailed description of the four column tests is provided in the following.

To validate the numerical model of the first columns type (type I), a full-scale reinforced concrete (RC) bridge column test was chosen. This test was performed on the NEES Large High-Performance Outdoor Shake Table located at UCSD's Englekirk Structural Engineering Center. The RC cantilever column was designed according to Caltrans seismic design specifications and was supported on a fixed foundation. Fig. 4 shows the test specimen and the setup for the experiment. The numerical modeling parameters, shown in Table 1, are according to the

Table 1
Parameters used in the OpenSees model for the UCSD column test.

Parameters	Values
Diameter of the column	1.22 m (4 ft)
Column height	7.31 m (24 ft)
Longitudinal reinforcements	18 #11
Transverse reinforcements (hoops)	Double #5 @152 mm (6 in)
Clear cover	51 mm (2 in)
Concrete strength	41.9 MPa (6.1 ksi)
Modulus of elasticity	22877 MPa (3317 ksi)
Concrete compressive strain at maximum compressive stress	0.0026
Yield strength of longitudinal steel	518.5 Pa (75.2 ksi)
Yield strain of longitudinal steel	0.0026
Ultimate strength of longitudinal steel	706.7 MPa (102.4 ksi)
Modulus of elasticity of longitudinal steel	196057 MPa (28426 ksi)
ϵ_{sh} of longitudinal steel	0.011
E_{sh} of longitudinal steel	5515.5 MPa (800 ksi)
ϵ_u of longitudinal steel	0.122
Yield strength of hoops	337.9 MPa (54.8 ksi)

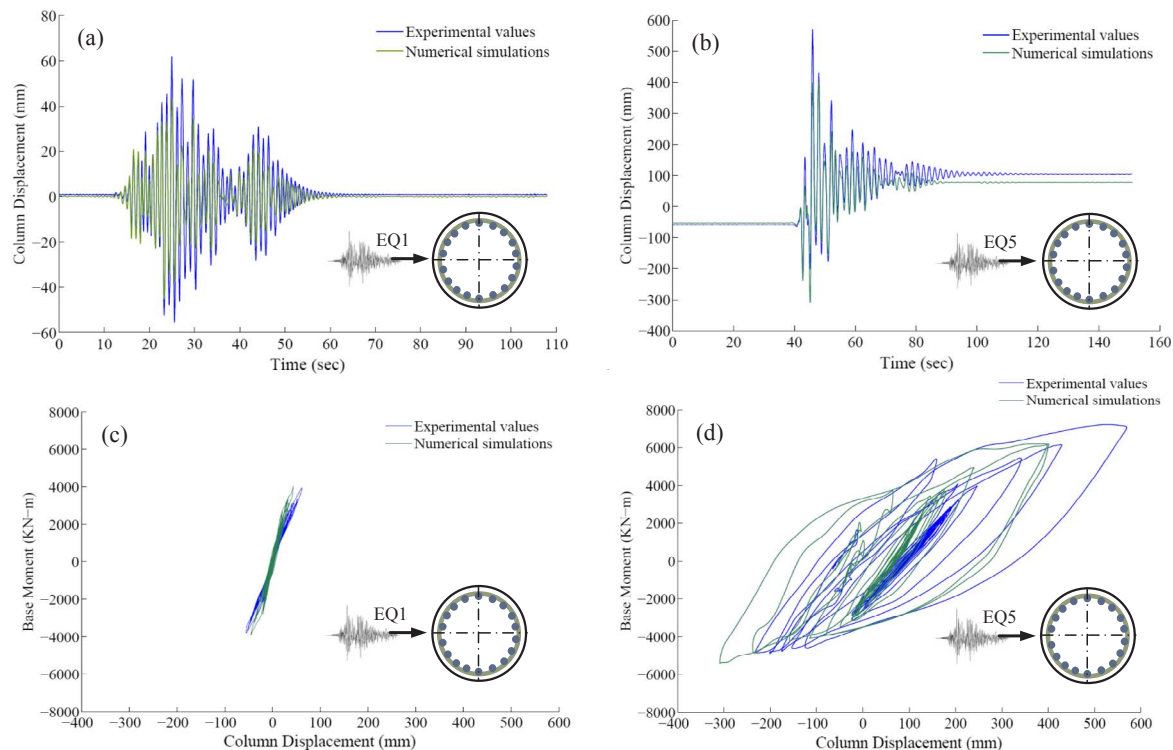


Fig. 5. Comparison of the results of the numerical simulations with those of the UCSD tests; (a) column top displacement (EQ1), (b) column top displacement (EQ5), (c) bending moment at column base (EQ1), and (d) bending moment at column base (EQ5).

provided values in the published report [26] regarding to the UCSD tests. The details of the column design and reinforcement are provided in Fig. 4. The specimen was subjected to six ground motions (Fig. 4) simulated by a shake table at UCSD. Similarly, the column's numerical model was subjected to the same set of motions. Nonlinear time history analysis was performed in OpenSees, and dynamic responses of the numerical model were captured. The responses include the column top displacement, the shear force at the base, and the bending moment at the column base. The response comparison of the full-time history analysis (Fig. 5) confirms that the analytical and experimental results are in agreement.

To validate the numerical models of column Types II and III, full-scale RC bridge column tests by Tanaka and Park [11], and Sanchez et al. [16] were chosen, respectively. The oblong cantilever column tested by Tanaka and Park [11] was designed according to the column provisions in the New Zealand concrete design code [27]. Sanchez et al. [16] constructed flared and prismatic columns according to Caltrans design code. Figs. 6 and 7 show the detailing of the column designs. In both studies, the columns were subjected to constant axial loads and cyclic horizontal loadings (Figs. 6 and 7). In the oblong cantilever column test, the cyclic horizontal load imposed on the specimen included one elastic cycle corresponding to a displacement ductility factor $\mu_d = \pm 0.75$ and two cycles for each of the factors $\mu_d = \pm 2, \pm 4, \pm 6, \pm 8$. In the other test, the displacement ductility factors used for applying the cyclic lateral loads were $\mu_d = \pm 1, \pm 1.5, \pm 2, \pm 3, \pm 4, \pm 5, \pm 6$ and $\mu_d = \pm 0.56, \pm 0.86, \pm 1.15, \pm 1.72, \pm 2.30, \pm 2.88, \pm 3.45$ for the prismatic and flared column, respectively. These experiments were simulated in OpenSees using similar cyclic loadings and performing cyclic pushover analysis. Then, the numerical results were compared with the experimental data. As shown in Fig. 8, the numerical simulations are fairly able to predict the real columns' performance.

The validation process indicates that the numerical modeling technique used in this study can provide a realistic behavior model for bridge columns with various shapes. In the following section, a typical

bridge column is modeled with the commonly used structural characteristics and its seismic performance is evaluated by varying the column shape.

3. Analytical evaluation of the columns' performance

This section provides an investigation of the columns behavior under both monotonic pushover and cyclic lateral loading. A general method of pushover analysis about the longitudinal and transverse axes was applied. The columns were assumed to be cantilevers subjected to constant axial loads equal to ten percent of their axial capacity ($f'_c A_g$).

The input parameters for the tested columns are presented in Table 2. A detailed plan review of existing bridges in California was conducted to extract the probability distributions of the required modeling parameters. These distributions are used in the bridge fragility analysis presented in the next section while the mean values of the modeling parameters (Table 2) are selected for the analysis of the columns in the current section. Four main cases, circular prismatic (CP), rectangular prismatic (RP), oblong prismatic (OP), and flared columns (FL), are considered in this study. The dimensions used in this section are the most common ones, based on review of the California bridge inventory. The bridge design details manual lists three standard column sizes as 4, 5.5, and 7 feet (1.2, 1.7, and 2.1 m) for an equivalent circular column. Reviewing the existing bridge plans revealed that the majority of circular single columns have a 5.5 feet (1.7 m) diameter and the majority of circular multi-column bents have a 4 feet (1.2 m) diameter. Similarly, the other cross-section dimensions were selected based on the existing bridge population. The possible number of columns for a multi-column bent bridge includes: two and three columns for bridges designed before 1970 and two to five columns for bridges designed after 1970. The column cross-section areas are approximately similar in the four considered cases. In order to have a fair comparison of only the effect of column shapes, it is essential to keep all structural characteristics such as reinforcement ratios and column height the same. Axial and moment capacities were similar between shapes to make a fair

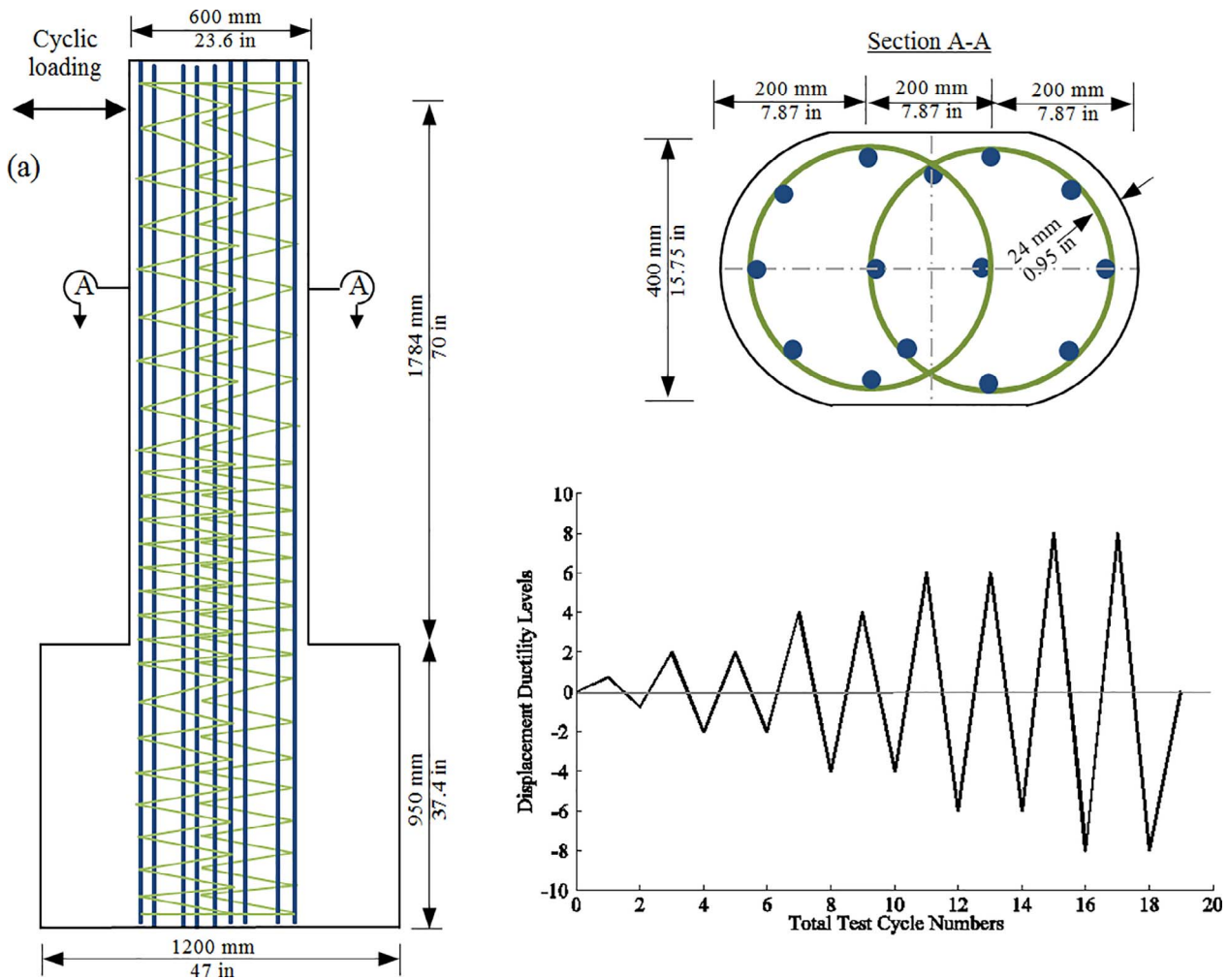


Fig. 6. Layout of the oblong columns tested by Tanaka and Park [111]; (a) Details of the column design, (b) Reinforcement arrangement, (c) Displacement ductility levels.

comparison. In order to account for the differences in bridge design code, separate analyses were performed for the specifications of bridges designed before and after 1970.

First, monotonic pushover analysis was conducted on the columns in both longitudinal and transverse directions of the columns. As shown in Fig. 9, two different patterns can be observed based on the direction of applied load, the arrangement of the longitudinal reinforcements, and the geometry of the confined concrete. In the longitudinal direction (Fig. 9), the rectangular cross-section shows the highest strength because the steel reinforcement is arranged at the farthest distance from the center which increases the moment of inertia of transformed section and, subsequently, the stiffness and strength. Two additional cross-section shapes with similar modeling properties and cross-sectional area were analyzed to verify the comparisons. One (SP in Fig. 9) is a square cross-section shape, and the other (36 × 48 rectangle, ERP in Fig. 9) is a rectangular cross section with dimensions between the square (SP) and original rectangular (RP) section. The strength and stiffness were shown to differ with shape with the lowest value corresponding to the circle (CP), then square (SP), and then to the two rectangles (RP and ERP). The two rectangular shapes exhibited the highest values for strength and stiffness as the cross-section is elongated in the longitudinal direction which changes the reinforcement arrangement and the geometry of the confined concrete. This phenomenon is reversed in the transverse direction. The oblong column has a response that is similar to the circular column in the longitudinal direction and the rectangular column in the transverse direction, due to the nearly similar arrangement of the rebar. The columns with flares

display higher resistance (i.e. higher strength and stiffness) than circular columns in both directions. That is the result of keeping the details of the non-flared sections of the flared column (from footing to half of the column height, Fig. 3b) identical to those of the prismatic columns, while the flared sections include an additional layer of reinforcement, similar to the layout shown in Fig. 7, and the cross-section dimension increases along the column height. Clearly, circular columns have identical responses in both directions because of the symmetry of the shape and the reinforcement. Additionally, increasing the reinforcement ratio while decreasing the confinement spacing enhances the load-carrying capacity of the column during deformations.

Second, a cyclic pushover analysis was performed on the columns to examine the hysteretic loop. The displacement cycles are defined based on the yield displacement of the longitudinal reinforcements. The yield displacement was calculated using the deformation components including flexural deformation, bar slip, and shear deformation. Their contributions in the yield displacement experienced by a column specimen can be represented as $\Delta_y = \Delta_{flexural} + \Delta_{slip} + \Delta_{shear}$, and each of these deformations can be calculated based on empirical equations [28]. The highest contribution corresponds to the flexural deformation that emerges when a moment load is generated in the column, and a lateral displacement occurs at the end of the column. For a column that is considered to be fixed at both ends against rotation, a linear variation in curvature over the column height is assumed, and the flexural displacement contribution in the yield displacement can be calculated as $\Delta_{flexural} = L^2\Phi_y/6$, where L and Φ_y are the column height and the curvature at the yield initiation point of the longitudinal reinforcements.

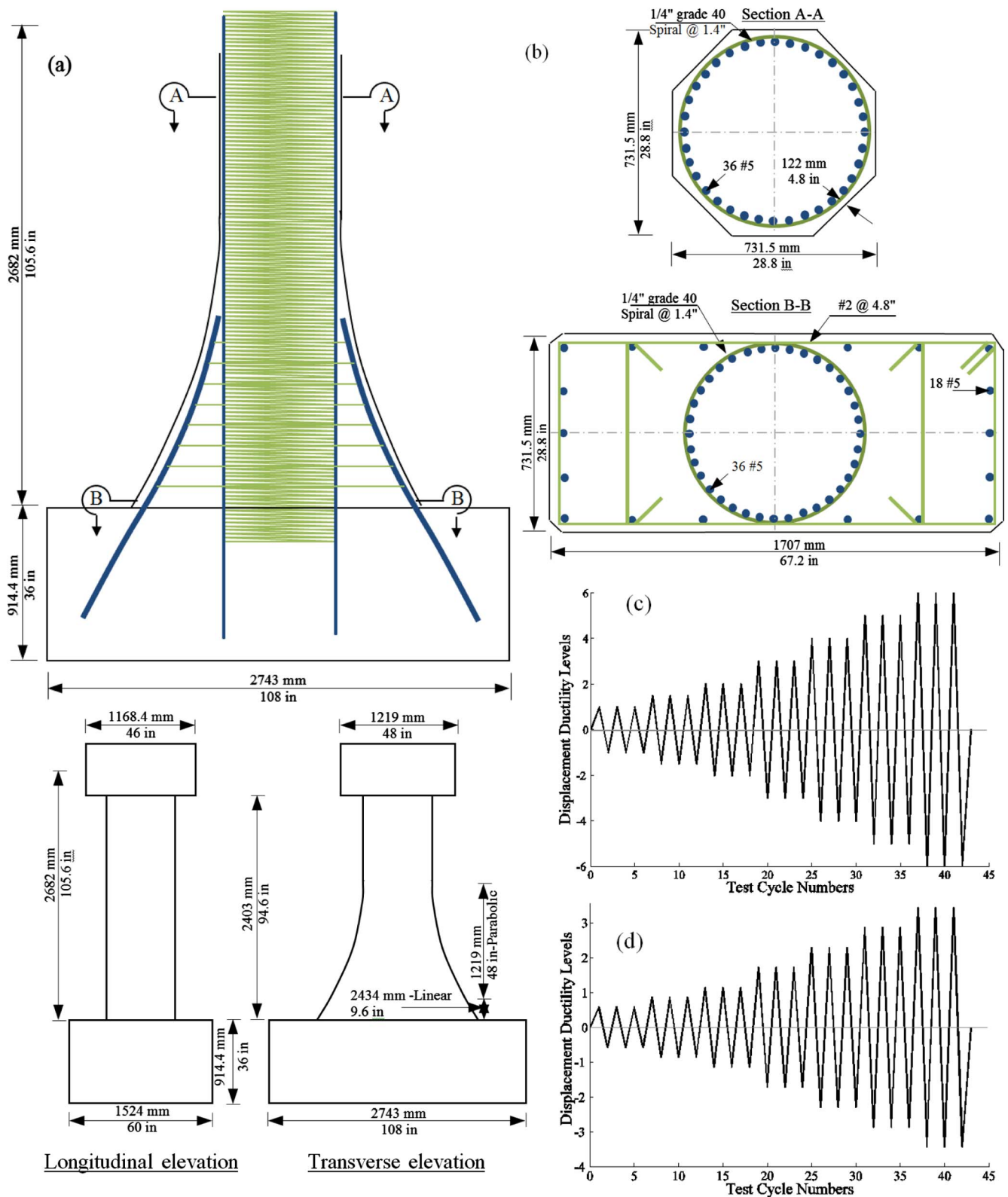


Fig. 7. Layout of the flared column tested by Sanchez, et al. [16]; (a) Details of the column design (inverted column), (b) Reinforcement arrangement, (c) Displacement ductility levels for prismatic column, (d) Displacement ductility levels for flared column.

The contribution of the shear and slip deformation are less than the flexural deformation; however, they will be counted in this study. The contribution of these deformations can be calculated using $\Delta_{shear} = 2M_y/GA_v$ and $\Delta_{slip} = Ld_B F_{YL} \Phi_y / 8u$, where M_y and A_v are the moment at first yield of the longitudinal reinforcement and the shear

area of the column section, d_B and F_{YL} are the diameter and the yield stress of the longitudinal reinforcements, and $u = 6\sqrt{f'_c}$ is the bond stress between the longitudinal reinforcement and the footing. The calculation of the total yield displacement requires estimations for Φ_y and M_y , using the moment-curvature relationships. This relationship

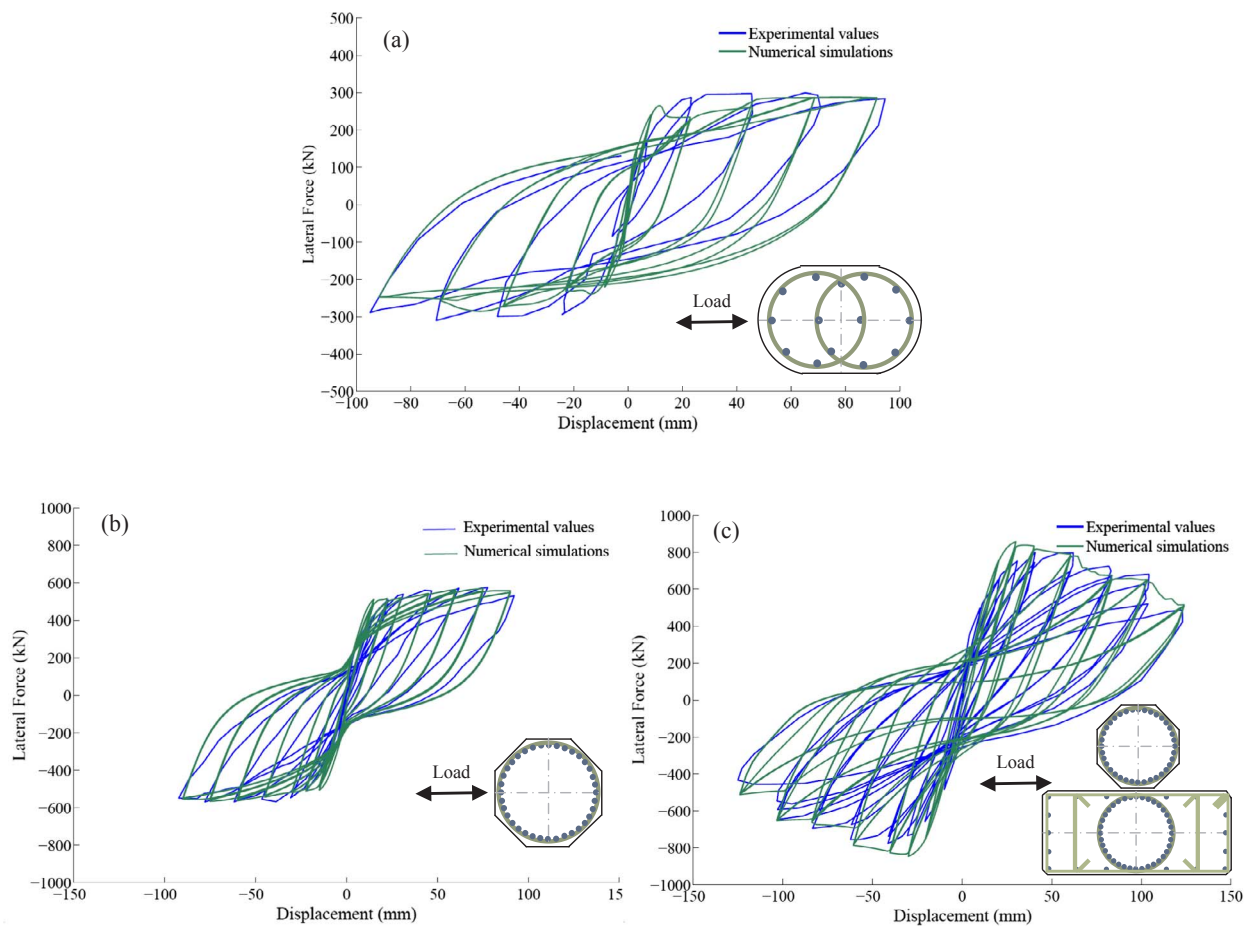
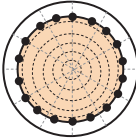
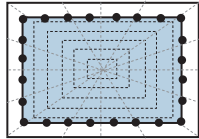
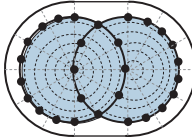
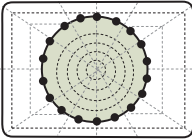


Fig. 8. Comparison of the lateral force versus lateral displacement hysteresis loops for: (a) oblong column (Fig. 6), (b) prismatic column, and (c) flared column (Fig. 7).

Table 2
Geometric parameters used in modeling cantilever columns for pushover analysis.

Parameters	Column name			
	CP	RP	OP	FI
Cross-section				
Type	I	II	II	III
Cross-section dimensions (in)				
Single column	66	36 × 96	48 × 72	66 & a = 2' 9"
Multi-columns (≥ 2)	48	36 × 48	36 × 48	48 & a = 2'
Cross-section dimensions (mm)				
Single column	1676.4	914.4 × 2438.4	1219.2 × 1828.8	1676.4 & a = 838.2
Multi-columns (≥ 2)	1219.2	914.4 × 1219.2	914.4 × 1219.2	1219.2 & a = 609.6
Column height				
Pre-1970 (ft)	21.5	21.5	21.5	21.5
Pre-1970 (m)	6.55	6.55	6.55	6.55
Post-1970 (ft)	24.0	24.0	24.0	24.0
Post-1970 (m)	7.32	7.32	7.32	7.32
Longitudinal reinforcement (%)				
Pre-1970	1.9	1.9	1.9	1.9
Post-1970	2.35	2.35	2.35	2.35
Transverse reinforcement				
Pre-1970	#4 @ 12"	#4 @ 12"	#4 @ 12"	#4 @ 12"
Post-1970	#4 @ 3"	#4 @ 3"	#4 @ 3"	#4 @ 3"

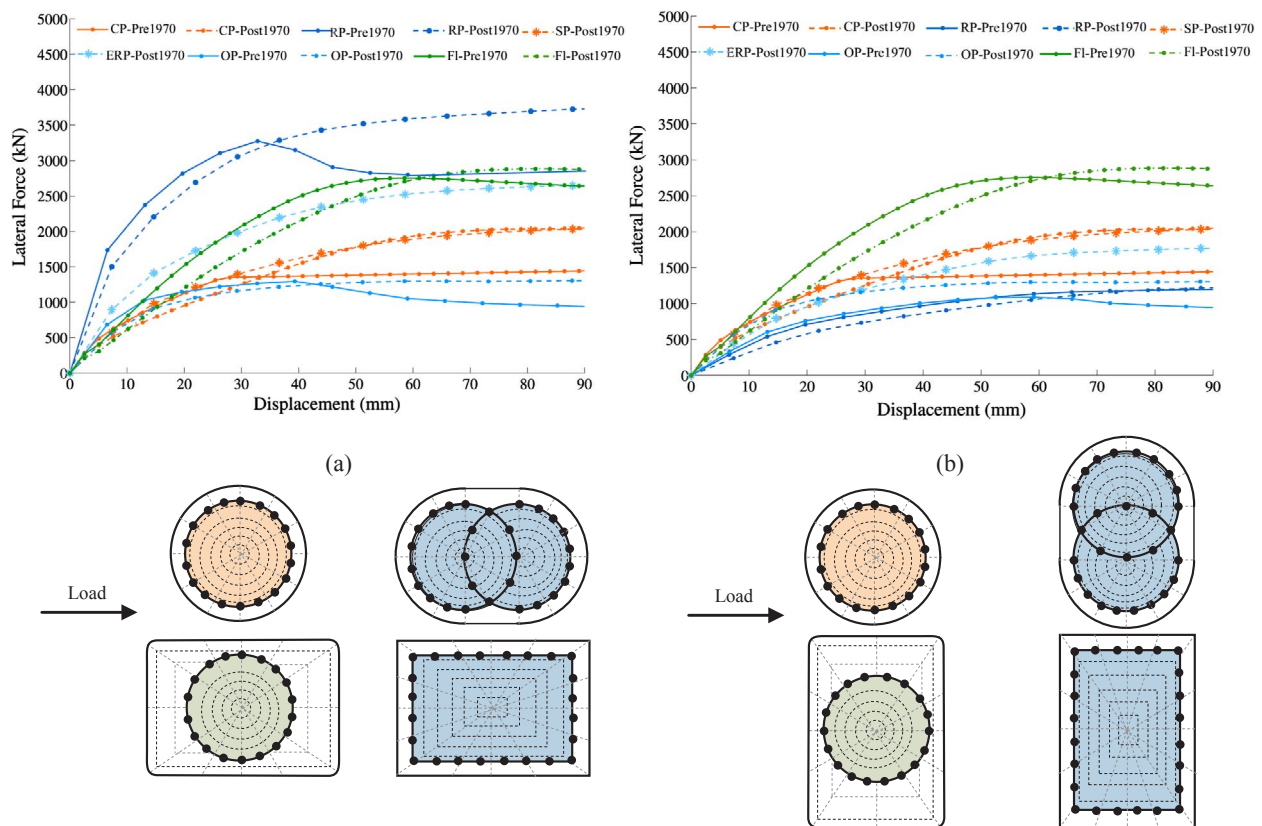


Fig. 9. Comparison of monotonic pushover analysis of the considered columns (Table 2) in this study in (a) longitudinal and (b) transverse directions.

is determined based on an OpenSees standard section analysis that relies on the assumption that plane sections remain plane. Based on the calculated yield displacements, the cyclic levels were set to be $\Delta = \pm 0.257, \pm 0.514, \pm 0.771, \pm 1.03, \pm 1.54, \pm 2.06, \pm 2.57, \pm 3.6, \pm 4.6, \pm 5.65, \pm 6.68, \pm 7.71$ (in) shown in Fig. 10, the cyclic behavior pattern across different cross-section shapes is similar to the observations from the monotonic pushover analysis (Fig. 9b). However, the strength degradation can be analyzed in the cyclic testing. This degradation happens at earlier levels in the flared columns, while it only occurs at the latest cycles for the other column shapes. The circular column shows a smooth degradation that increases during the last few cycles, whereas the rectangular and oblong columns display a drastic decrease in the strength in the last cycle.

In the following section, the influence of various column shapes on the seismic performance of the bridges is evaluated.

4. Seismic analysis

A hypothetical box-girder bridge with the structural properties of California bridges was modeled in three-dimensions in OpenSees. Table 3 provides a description of bridge class varieties that are considered in this study. The bridge layout and the backbone curves used in the components modeling are presented in Fig. 11. As shown in Fig. 11, each analysis needed to be conducted twice for the two types of rigid and seat abutments. A detailed plan review of the existing bridges in California was conducted to extract required data to consider uncertainties. Table 4 provides the probability distributions and associated parameters of the required modeling parameters such as the yield strength of the steel (f_s) and the unconfined standard compressive strength of concrete (f_c) which are considered as random variables. Interested readers are directed to the work of Soleimani [25] for a more detailed explanation of the modeling parameters. Similar to the analysis

provided in the previous section, the four cases of column shapes (CP, RP, OP, and FI) were considered in the bridge study. Additionally, two separate sets of analysis were performed in order to account for the variations in reinforcement ratios and column heights in design codes written before and after 1970.

Nonlinear Time History Analysis (NLTHA) was performed on the bridge models using Baker's suite of 160 ground motions [29]. These excitations have longitudinal and orthogonal components, and are randomly oriented to the longitudinal and transverse directions of the bridge models. The results of this analysis provided the peak seismic response for each of the bridge components. The peak responses were used to produce probabilistic seismic demand models (PSDM). A probabilistic seismic demand model (PSDM) is a regression model expressing the relationship between seismic demand (D) and ground motion intensity measure (IM). Based on this regression model, the median value of the seismic demand (S_D) can be estimated for a specific intensity measure as

$$S_D = a \cdot IM^b, \tag{1}$$

where a and b are the regression coefficients that are obtained by performing a regression analysis on $D-IM$ pairs. For this study, Sa-1.0 s (i.e. the spectral acceleration at 1.0 s) was chosen since it was determined as the optimal intensity measure for developing fragility curves of box-girder bridges [8]. Dispersion (β_{DIM}) is calculated based on

$$\beta_{DIM} = \sqrt{\frac{\sum_{i=1}^N (\ln(D_i) - \ln(S_D))^2}{N-2}}, \quad (N = \text{total number of data points}). \tag{2}$$

In order to generate fragility curves for the bridge system, the PSDM should be developed for each of the bridge components (e.g. columns, abutments, foundations). The bridge column vulnerability has a major

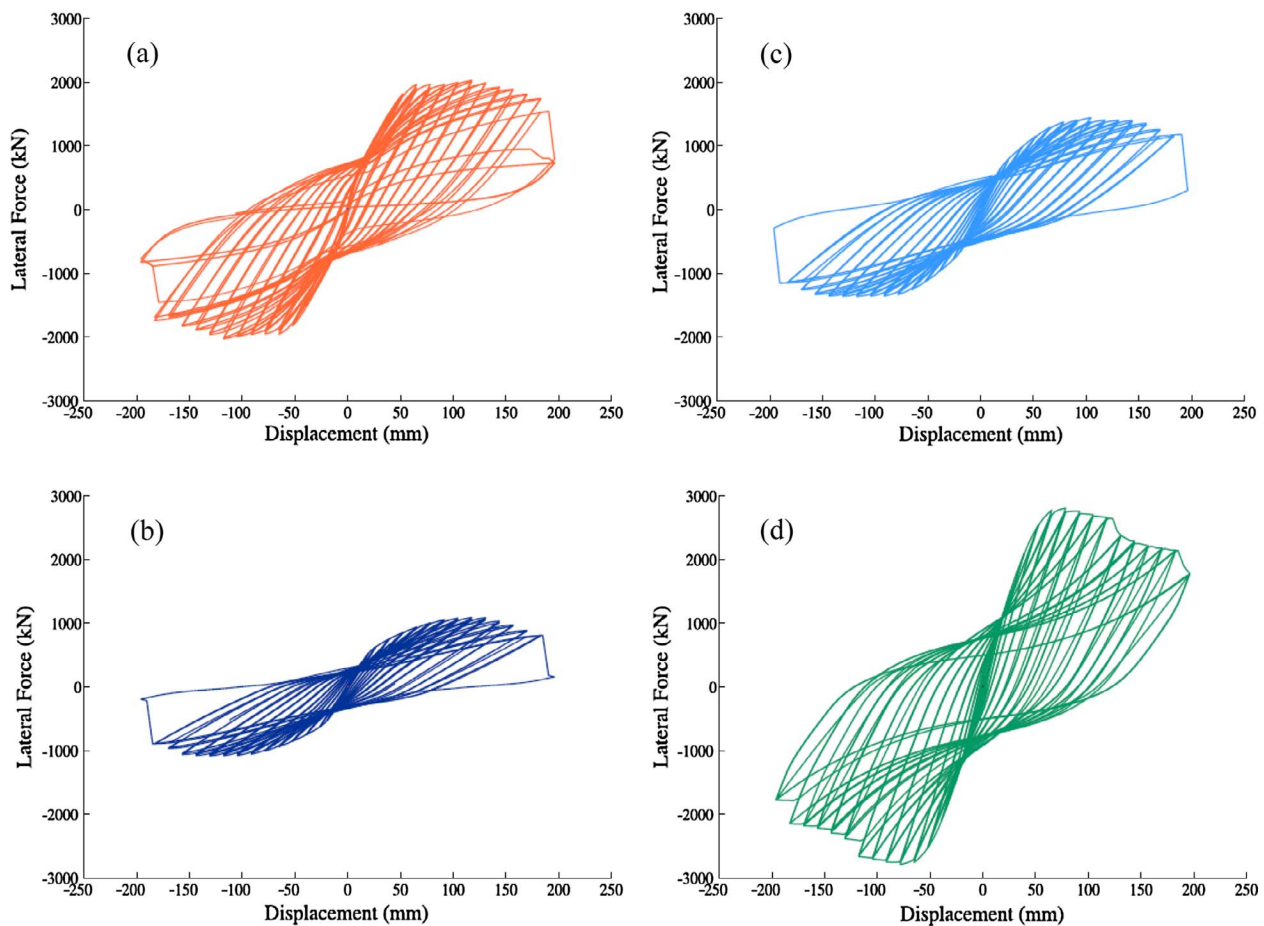


Fig. 10. Comparison of cyclic pushover analysis for (a) CP, (b) RP, (c) OP, and (d) FI columns listed in Table 2, in the transverse direction.

Table 3
Description of nomenclature for bridge classes considered in this study.

Nomenclature	Classification		
	Abutment	Design era	Number of columns per bent
DBSC	Rigid diaphragm (D)	Pre-1970 (B)	Single (SC)
SBSC	Seat abutment (S)	Pre-1970 (B)	Single (SC)
DBMC	Rigid diaphragm (D)	Pre-1970 (B)	Multiple (≥ 2) (MC)
SBMC	Seat abutment (S)	Pre-1970 (B)	Multiple (≥ 2) (MC)
DASC	Rigid diaphragm (D)	Post-1970 (A)	Single (SC)
SASC	Seat Abutment (S)	Post-1970 (A)	Single (SC)
DAMC	Rigid diaphragm (D)	Post-1970 (A)	Multiple (≥ 2) (MC)
SAMC	Seat abutment (S)	Post-1970 (A)	Multiple (≥ 2) (MC)

contribution to the overall bridge system fragility. As a result, column displacement ductility, defined as the ratio of the ultimate displacement to the yield displacement, is assessed in this study. Figs. 12 and 13 depict the two-parameter lognormal probability distribution of the column ductility based on the ground motion intensity measure. Each row in Figs. 12 and 13 corresponds to the PSDM plots of a specific bridge type mentioned in the figure captions. The description of the nomenclatures used for the considered bridge classes in this paper can be found in Table 3. Moreover, each column includes the plots of a particular cross-section shape.

Among the developed PSDMs, those of the oblong cross-sections have noticeably different slopes. More specifically, in all bridge types (Figs. 12 and 13), the slopes of the oblong column models are the lowest between the considered column shapes. In contrast, the highest slopes of the PSDMs belong to the flared shape columns, in almost all cases. No specific pattern is observed between circular and rectangular column shapes. These findings are not restricted to a particular abutment type, number of columns per bent, or the era when the bridge was designed.

The developed PSDMs were used to establish the fragility curves. This research study also aims to investigate the effect of column shapes on the fragility analysis of a bridge, and follows the work of Nielson [4] and Ramanathan [8] to evaluate the fragility of bridge components at four different damage states: slight, moderate, extensive, and complete. Table 5 provides HAZUS [30] definitions of the four bridge damage states. At a chosen intensity measure, the probability that the seismic demand (D) of a component exceeds its capacity (C) can be assessed by fragility curves. A lognormal distribution of demand and capacity is assumed [31], and the probability of reaching or exceeding a specific damage state for a particular component is then estimated with the use of the probability equation

$$P[D > C|IM] = \Phi \left[\frac{\ln(S_D/S_C)}{\sqrt{\beta_{DIM}^2 + \beta_C^2}} \right], \tag{3}$$

where, S_C is the median estimate of the capacity, β_C is the dispersion of the capacity, and $\Phi(\cdot)$ is the standard normal cumulative distribution function.

The capacity limit states used for the displacement ductility and the other demand parameters were derived based on previous experimental results [25]. Figs. 14 and 15 demonstrate the fragility curves of bridge

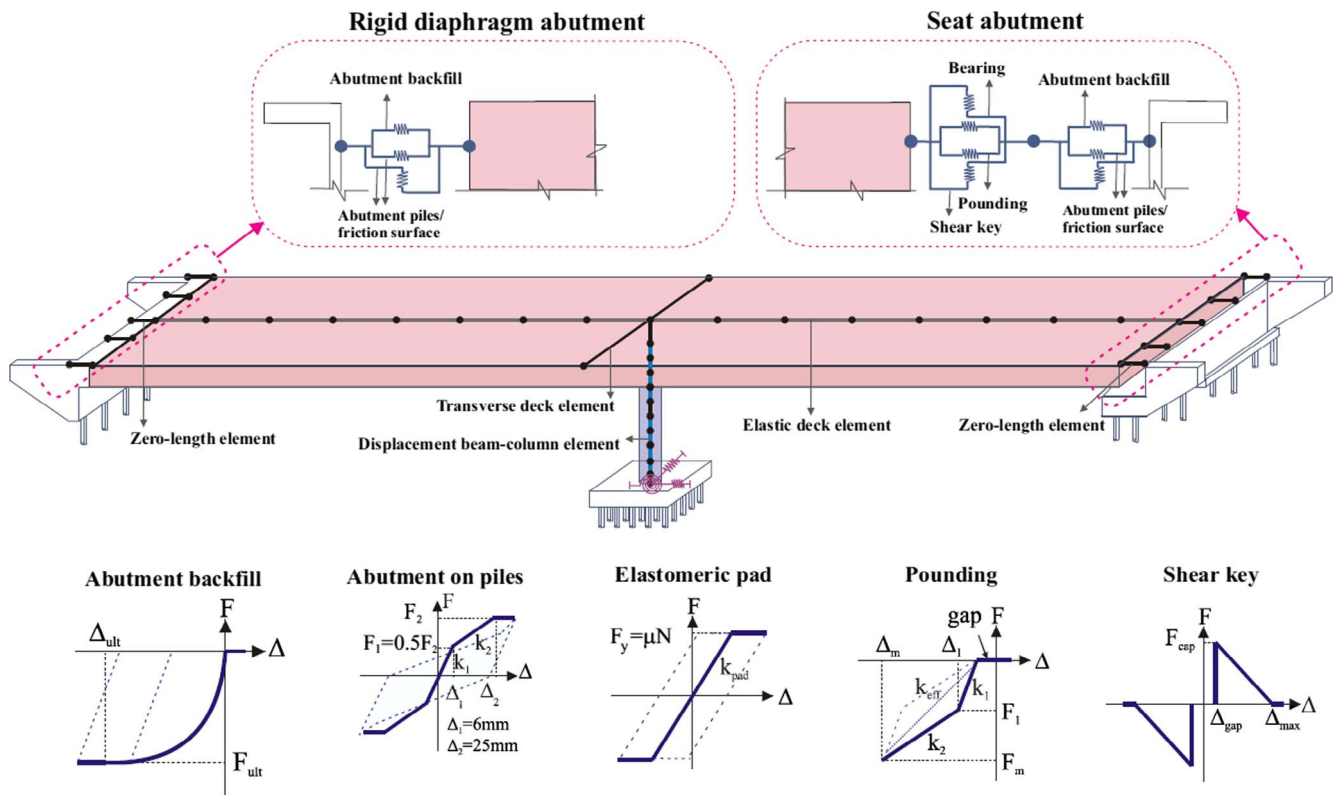


Fig. 11. Numerical modeling of various bridge components.

Table 4
Uncertainty distribution considered in the bridge models [25].

Parameter	Distribution		
	Type	μ	σ
Concrete compressive strength (MPa)	Normal	29.03	3.59
Reinforcing steel yield strength (MPa)	Lognormal	465.0	37.30
<i>Span length (mm)</i>			
Two-span	Lognormal	31775	8738
<i>Deck width (mm)</i>			
Single column bent	Lognormal	9780	1980
Multi-column bent	Lognormal	11970	2418
<i>Abutment backwall height (mm)</i>			
Diaphragm abutments	Lognormal	3234	488
Seat-type abutments	Lognormal	2186	441
<i>Abutments on piles – lateral capacity/deck width (N/mm)</i>			
Diaphragm abutment	Lognormal	1120	404
Seat-type abutment	Lognormal	1498	540
<i>Elastomeric bearing pad</i>			
Stiffness per deck width (N/mm/m)	Lognormal	908	327
Coefficient of friction for bearing pad	Normal	0.30	0.10
<i>Gap (mm)</i>			
Longitudinal (btw. deck & abutment wall)	Lognormal	23.5	12.5
Transverse (btw. deck and shear key)	Lognormal	12.8	2.58
Mass factor	Uniform	1.25	0.007
Damping	Normal	0.045	0.0125
Acceleration for shear key capacity (g)	Lognormal	1.00	0.20
<i>Piles translational stiffness (N/mm)</i>			
1% long. rebar	Normal	297716	140101
3% long. rebar	Normal	245178	105076
<i>Piles rotational stiffness (N-m/rad)</i>			
1% long. rebar	Normal	4.5×10^9	1.1×10^9
3% long. rebar	Normal	6.8×10^9	1.1×10^9

columns when different types of column shapes are used in the models. Each plot depicts the column vulnerability at slight, moderate, extensive, and collapse damage state. The plots that are placed in the same row correspond to an identical bridge type with the four considered column shapes, CP, RP, OP, and FI. Hence, each column in the figures shows the fragility curves for various bridge types (e.g. different abutment types) but similar column shapes.

As is shown in Figs. 14 and 15, the column seismic vulnerability of seat-type abutment bridges is generally higher than that of integral-type ones. Comparing the fragilities of each row reveals that the oblong column shapes are less fragile than any other column shape at four damage states. The results show that when oblong columns are used, the seismic vulnerability of the column decreases in bridges with either seat- or rigid-type abutments. In other words, oblong bridge columns are the least vulnerable due to the more effectively confined area of the cross-section. Although flared columns represent a higher strength compared to prismatic in the pushover analysis, they are more prone to damage in the time history analysis. In particular, the fragility curves of bridge columns indicate a higher probability of damage for bridges consisting of flared columns in comparison to those made of straight columns. This is the result of the inconsistent cross-section along the column height and more specifically the elongation of the cover concrete area.

Another finding is that at low and medium damage levels for bridges with multiple columns per bent, there is not a noticeable difference observed between the performances of columns with various shapes. However, these performances become more distinctive at the higher damage levels. This is because the column shape plays a more significant role in providing the column's stiffness at larger displacement capacities and, accordingly, at larger deformations. More specifically, the column shape affects the reinforcing details, which define the column ductility demands and the seismic resistance.

The failure probabilities of bridge columns are presented in Table 6. The likelihood of observing damage can be compared at any level of

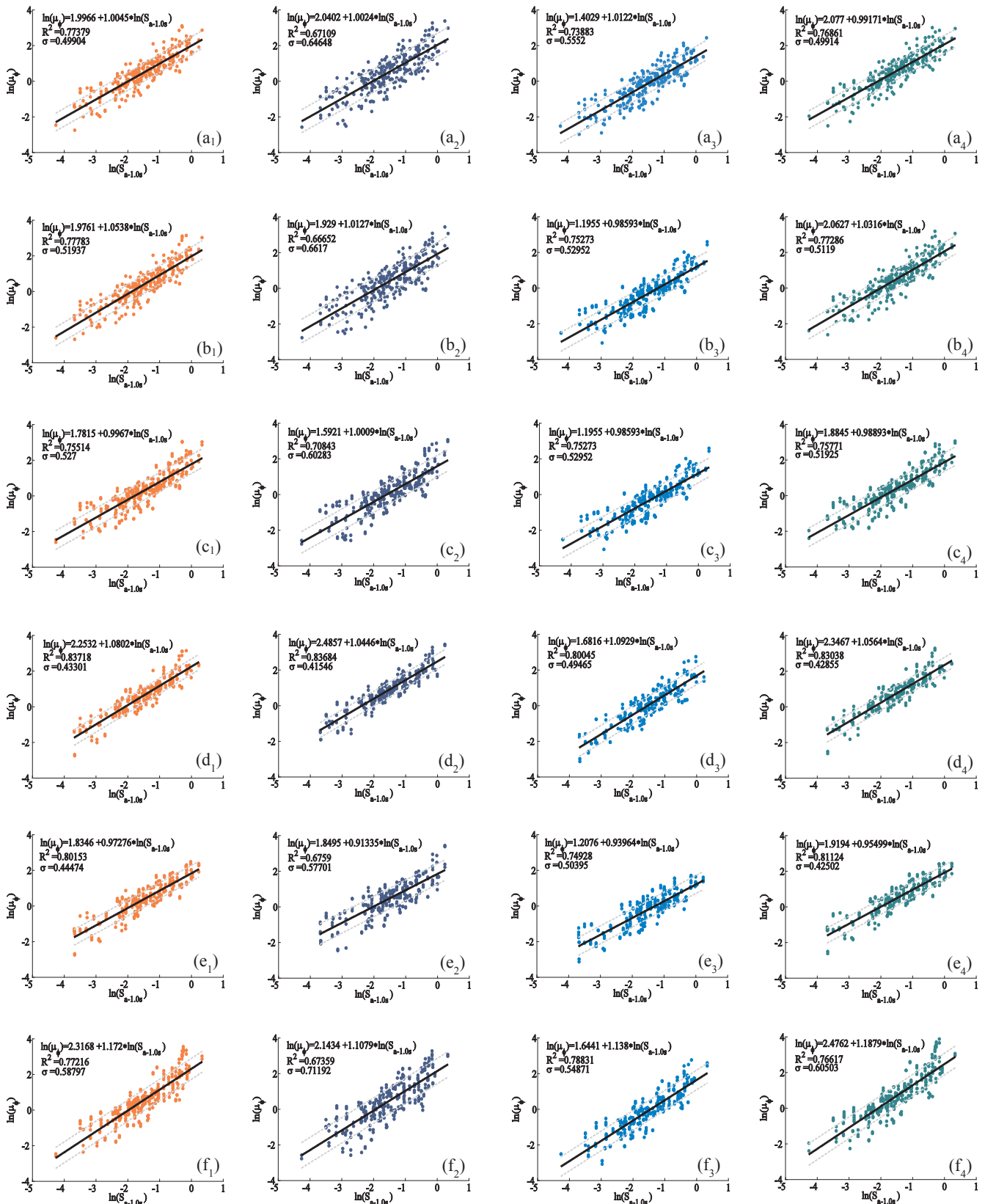


Fig. 12. Probabilistic seismic demand models for column displacement ductility of bridges: (a) DBSC, (b) SBSC, (c) DBMC, (d) SBMC, (e) DASC, (f) SASC, ● 1-circular, ● 1-rectangular, ● 1-oblong, ● 1-flared shape (Note: refer to Table 3 for the list of nomenclatures).

ground motion intensity; however, as an example, 0.5g is selected in the following. Comparing cases 1 to 4, at a spectral acceleration of 0.5g, probabilities of moderate damage to the bridge column with circular,

rectangular, oblong, and flared shapes are 81.8%, 73.3%, 57.8%, and 84.9%, respectively. For the same bridge type and at the same level of ground motion intensity, there is a 65.6%, 57.9%, 41.5%, and 69.3%

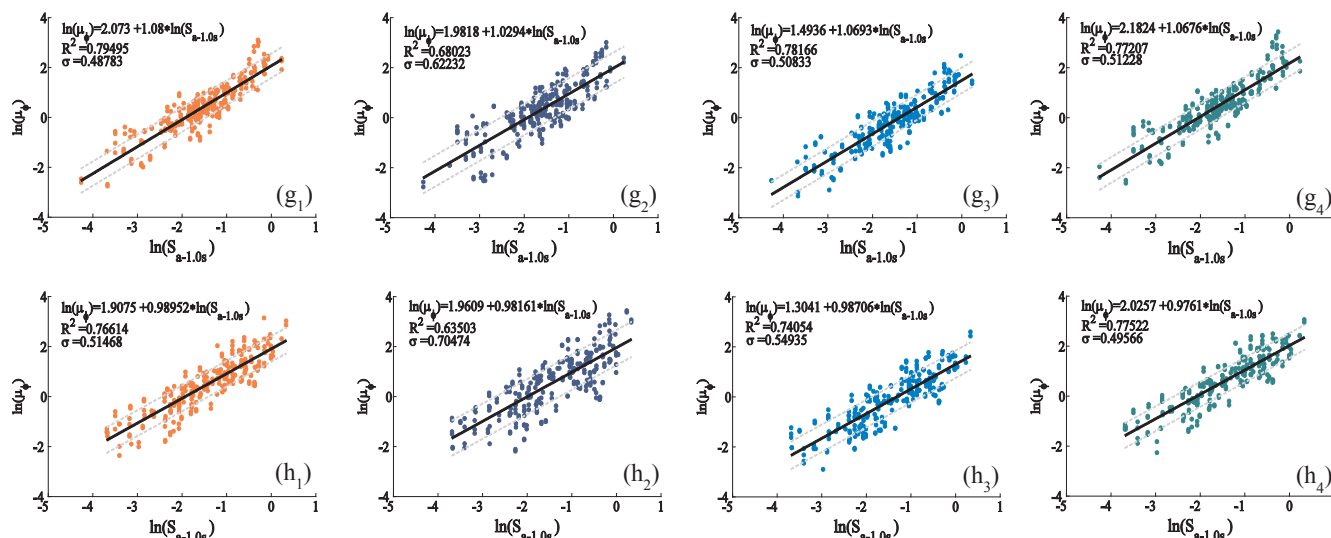


Fig. 13. Probabilistic seismic demand models for column displacement ductility of bridges: (g) DAMC, (h) SAMC, ● 1-circular, ● 1-rectangular, ● 1-oblong, ● 1-flared shape (Note: refer to Table 3 for the list of nomenclatures).

Table 5
HAZUS definition of the four bridge damage states.

Damage states	Definition of damage states
Slight	Minor cracking or spalling on any of these bridge components: column, abutment, shear key, hinge, and deck. However, the damage usually requires only cosmetic repair.
Moderate	Column experiencing moderate cracking (particularly shear cracking) and spalling, observing moderate movement of the abutment (< 50 mm), extensive cracking and spalling of shear keys, any connection having cracked shear keys or bent bolts, keeper bar failure without unseating, rocker bearing failure or moderate settlement of the approach.
Extensive	Column degrading without collapse, shear failure, significant residual movement at connections, major settlement approach, vertical offset of the abutment, differential settlement at connections, shear key failure at abutments.
Complete	Column collapsing and connection losing all bearing support, which may lead to imminent deck collapse, tilting of substructure due to foundation failure.

possibility of observing extensive damage in bridge columns with circular, rectangular, oblong, and flared shapes, respectively. Since the circular column shapes are used in the majority of bridges (approximately 53% of California’s box-girder bridges), the performance of the rectangular, oblong, and flared columns are compared to the performance of the circular column. This comparison is provided as the absolute relative error ϵ in Table 6 and Fig. 16. The results show that, at slight, moderate, extensive, and collapse damage levels, the maximum variations (relative errors) which are 25.02%, 30.78%, 38.42%, and 62.38% occur for the oblong cases.

Fig. 17 demonstrates the bridge system and components fragility curves. It was shown that, in all cases, the most vulnerable components significantly affect the seismic fragility of the bridge system. In this study, it is observed that for the considered bridge types and column shapes, columns dominate the fragility of the whole bridge (as also noted by recent studies [25,32]), and hence similar trends are observed in analyzing the system fragility curves as those of the column curves. However, the bridge system is more fragile than any of its components. The median and dispersion of the fragility functions for the four damage states are presented in Table 7. The first column of the table shows the bridge classes that are consistent with the ones assigned to the bridges in Tables 3 and 6.

According to the generated fragility curves for bridges with integral abutment type, bridge system fragilities can be sorted based on their column shapes as oblong, rectangular, circular, and flared, with oblong columns showing the lowest fragility. Similarly, the ranking for bridges with seat-type abutments lists as oblong, circular, rectangular, and flared columns. However, in both types of abutments, the difference between the system fragilities of bridges with oblong columns is more noticeable than the other considered shapes. This difference is

enhanced at higher levels of damage. A closer look at the bridge component and system fragility curves shows that the abutment seat has a lower fragility probability for bridges with oblong columns than for any of the other considered column shapes. A similar behavior is observed for the displacement of the elastomeric bearing.

5. Conclusions

Fragility analysis is a powerful tool for the reliability and risk assessment of structures, and is extensively applied by researchers to predict the extent of probable seismic damage to bridges with standard configurations. The seismic fragility analysis of many types of highway bridges in the United States has been explored. However, most of the previous studies have focused on bridges constructed with circular or rectangular columns, and hence the effect of column shape on the fragility assessment of a bridge system is not yet well-known.

The effect of common bridge column shapes on the seismic performance of bridges was analytically assessed in this study through the pushover analysis of individual columns and fragility analysis of a hypothetical bridge. The structural characteristics of the existing box-girder bridges located in California were utilized to generate finite element models. Three-dimensional numerical models of a typical bridge column with various common shapes including circular, rectangular, and oblong cross-sections as well as prismatic and flared columns were created in OpenSees. The numerical models were validated with the previous experiments and account for the uncertainties in modeling the bridge components. Then, the seismic assessments of typical bridge columns were conducted through a set of monotonic and cyclic pushover analysis. Next, a three-dimensional numerical model of a typical box-girder bridge was made with the considered variety of

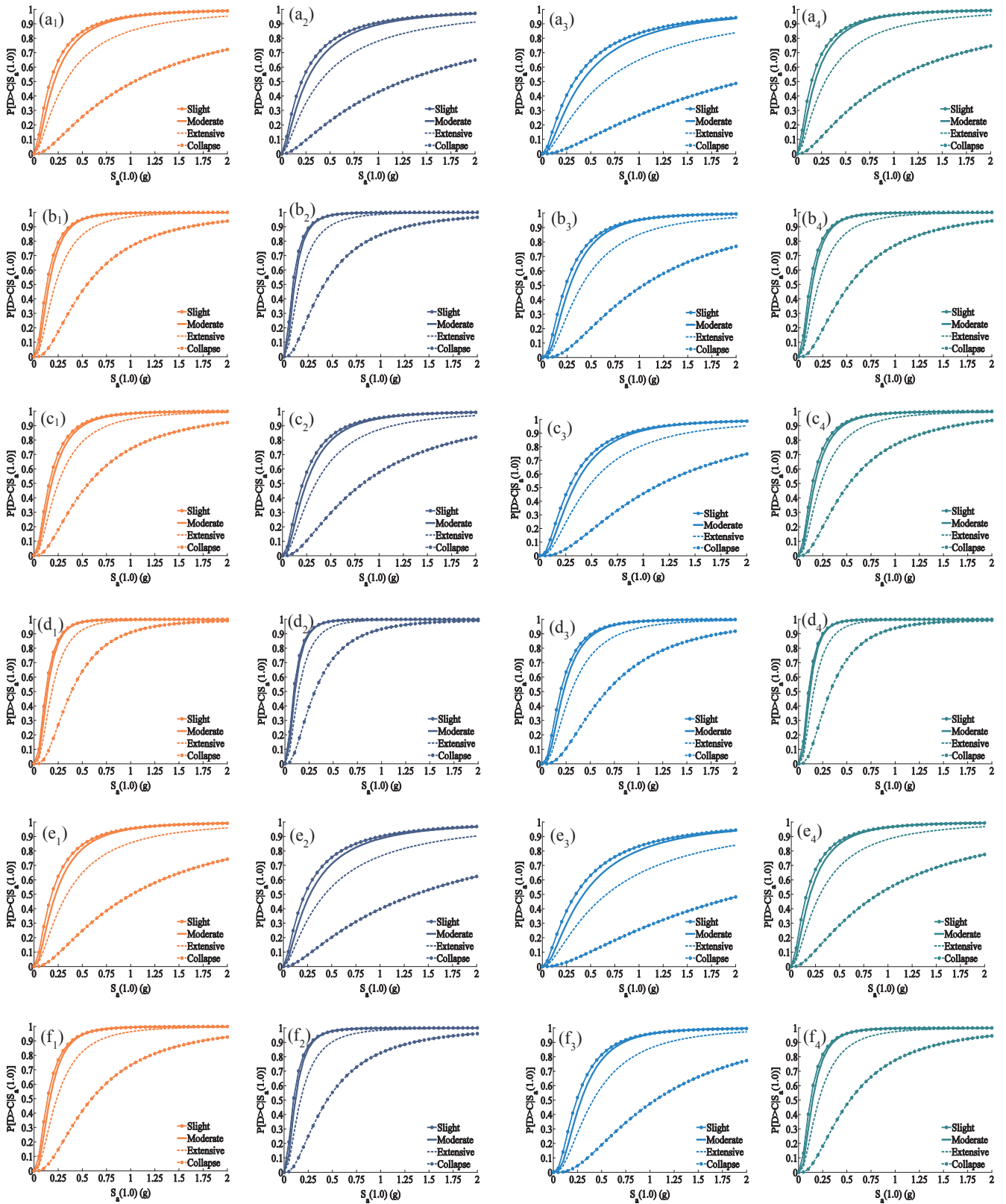


Fig. 14. Fragility curves of the columns for bridges: (a) DBSC, (b) SBSC, (c) DBMC, (d) SBMC, (e) DASC, (f) SASC, ● 1-circular, ● 1-rectangular, ● 1-oblong, ● 1-flared shape (Note: refer to Table 3 for the list of nomenclatures).

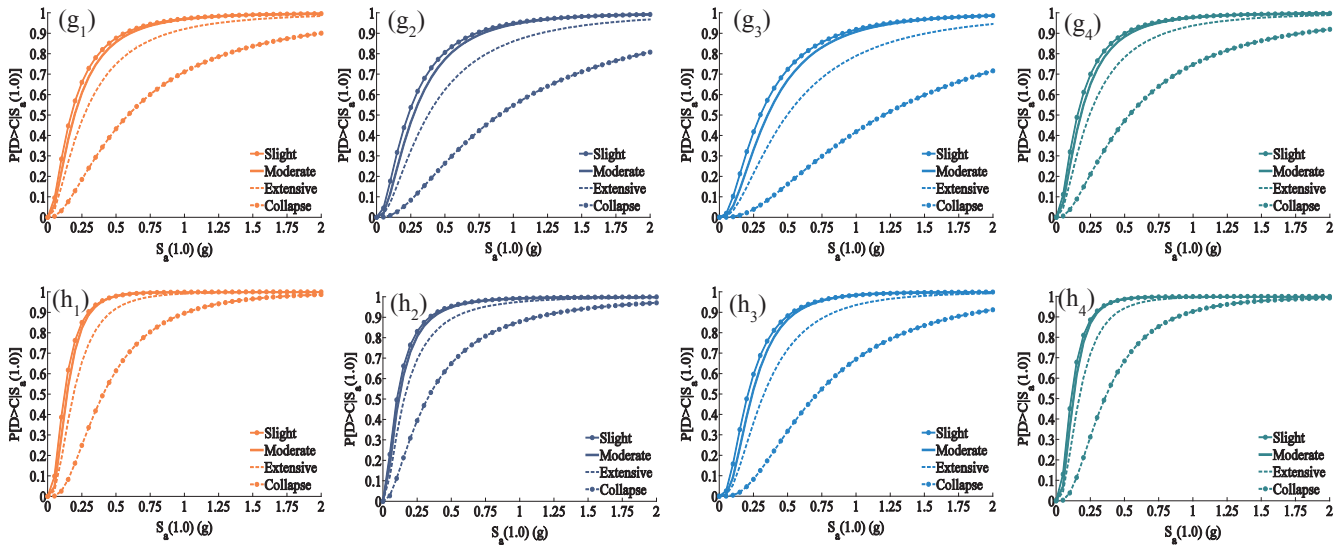


Fig. 15. Fragility curves of the columns for bridges: (g) DAMC, (h) SAMC, ● 1-circular, ● 1-rectangular, ● 1-oblong, ● 1-flared shape (Note: refer to Table 3 for the list of nomenclatures).

Table 6
Damage probabilities of the bridge columns at 0.5 g.

Case ^a	Figure	Column shape	Damage state							
			Slight		Moderate		Extensive		Collapse	
			P	ε (%)	P	ε (%)	P	ε (%)	P	ε (%)
DBSC	Fig. 14a ₁	CP	0.845	–	0.818	–	0.656	–	0.257	–
DBSC	Fig. 14a ₂	RP	0.774	8.46	0.733	10.46	0.579	11.82	0.227	11.49
DBSC	Fig. 14a ₃	OP	0.644	23.89	0.578	29.32	0.415	36.69	0.114	55.59
DBSC	Fig. 14a ₄	FI	0.871	3.00	0.849	3.81	0.693	5.66	0.286	11.16
SBSC	Fig. 14b ₁	CP	0.953	–	0.950	–	0.844	–	0.456	–
SBSC	Fig. 14b ₂	RP	0.980	2.88	0.981	3.29	0.915	8.48	0.585	28.42
SBSC	Fig. 14b ₃	OP	0.810	15.00	0.774	18.52	0.598	29.17	0.204	55.11
SBSC	Fig. 14b ₄	FI	0.960	0.77	0.960	1.01	0.860	1.96	0.473	3.78
DBMC	Fig. 14c ₁	CP	0.910	–	0.897	–	0.788	–	0.445	–
DBMC	Fig. 14c ₂	RP	0.827	9.12	0.797	11.18	0.655	16.80	0.297	33.26
DBMC	Fig. 14c ₃	OP	0.748	17.85	0.703	21.72	0.538	31.71	0.189	57.58
DBMC	Fig. 14c ₄	FI	0.927	1.83	0.918	2.26	0.816	3.61	0.479	7.67
SBMC	Fig. 14d ₁	CP	0.981	–	0.982	–	0.927	–	0.641	–
SBMC	Fig. 14d ₂	RP	0.988	0.66	0.989	0.65	0.951	2.62	0.730	13.84
SBMC	Fig. 14d ₃	OP	0.895	8.80	0.879	10.51	0.743	19.79	0.356	44.44
SBMC	Fig. 14d ₄	FI	0.989	0.74	0.990	0.76	0.952	2.68	0.722	12.58
DASC	Fig. 14e ₁	CP	0.843	–	0.814	–	0.648	–	0.249	–
DASC	Fig. 14e ₂	RP	0.755	10.38	0.710	12.77	0.551	14.92	0.203	18.49
DASC	Fig. 14e ₃	OP	0.632	25.02	0.564	30.78	0.399	38.42	0.103	58.44
DASC	Fig. 14e ₄	FI	0.870	3.24	0.850	4.36	0.693	6.92	0.288	15.89
SASC	Fig. 14f ₁	CP	0.945	–	0.942	–	0.825	–	0.415	–
SASC	Fig. 14f ₂	RP	0.977	3.37	0.978	3.81	0.904	9.60	0.553	33.28
SASC	Fig. 14f ₃	OP	0.814	13.88	0.778	17.43	0.593	28.13	0.190	54.18
SASC	Fig. 14f ₄	FI	0.961	1.74	0.961	1.97	0.860	4.34	0.470	13.33
DAMC	Fig. 15g ₁	CP	0.876	–	0.857	–	0.749	–	0.433	–
DAMC	Fig. 15g ₂	RP	0.806	7.97	0.773	9.83	0.624	16.77	0.264	38.98
DAMC	Fig. 15g ₃	OP	0.724	17.36	0.672	21.61	0.504	32.77	0.163	62.38
DAMC	Fig. 15g ₄	FI	0.899	2.63	0.883	3.07	0.783	4.49	0.472	9.17
SAMC	Fig. 15h ₁	CP	0.979	–	0.980	–	0.918	–	0.614	–
SAMC	Fig. 15h ₂	RP	0.954	2.56	0.949	3.13	0.892	2.90	0.673	9.62
SAMC	Fig. 15h ₃	OP	0.883	9.86	0.865	11.71	0.718	21.77	0.318	48.22
SAMC	Fig. 15h ₄	FI	0.986	0.72	0.987	0.79	0.942	2.60	0.684	11.36

^a Refer to Table 3 for the list of nomenclatures.

column shapes. Using a selected set of ground motions, nonlinear time history analysis was performed on the created models to derive structural responses. The seismic performance of the bridge models was evaluated by comparing their probabilistic seismic demands, the bridge column and the system fragility curves.

Assessment of the generated curves indicated the impact of column shapes on the bridge fragilities. Important conclusions are summarized as follows:

1. Among the considered column shapes, oblong and flared columns

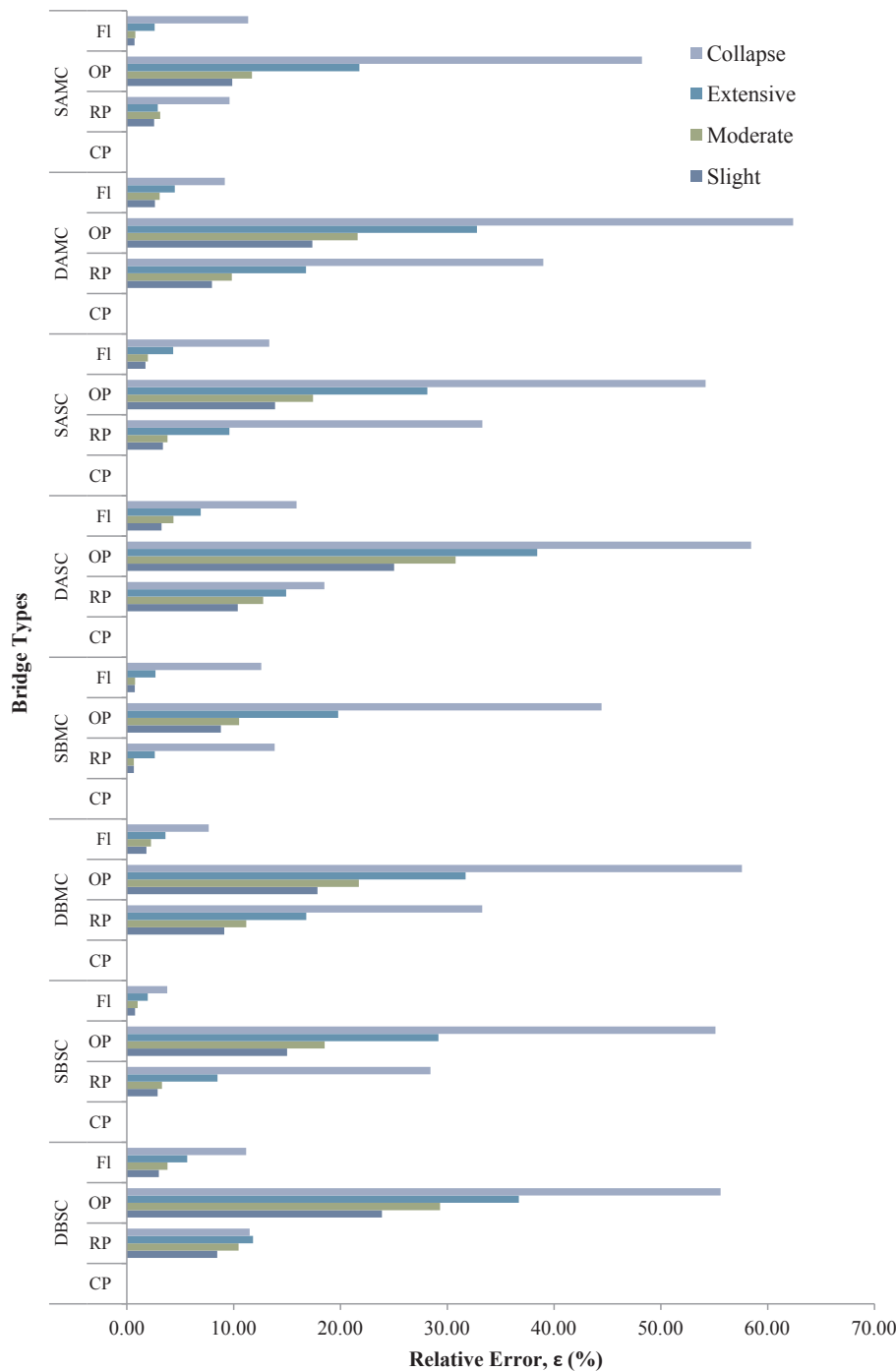


Fig. 16. Relative errors for damage probabilities of the bridge columns at 0.5 g (Note: refer to Table 3 for the list of nomenclatures).

indicated the lowest and highest vulnerability, respectively. This was more noticeable at higher levels of damage such as the extensive damage state.

2. Although bridges with seat abutments represented higher probability in the fragility analysis of the bridge column and system, similar trends were observed for the impact of column shapes on bridges with rigid and seat abutment types.
3. Additionally, it was observed that the findings were independent of the number of bridge columns per bent.
4. The cyclic tests comparisons showed that the strength degradation happened at earlier levels in the flared columns, while it only

occurred at the latest cycles for the prismatic columns.

5. Among the developed PSDMs, those of the oblong cross-sections had noticeably different slopes.
6. No specific pattern was observed on developed PSDMs comparing circular and rectangular column shapes.
7. In particular, the fragility curves of bridge columns indicated a higher probability of damage for bridges consisting of flared columns in comparison to those made of straight columns.
8. The performance comparison of the rectangular, oblong, and flared columns to the circular columns showed that the maximum variations occurred for the oblong cases at all damage levels.

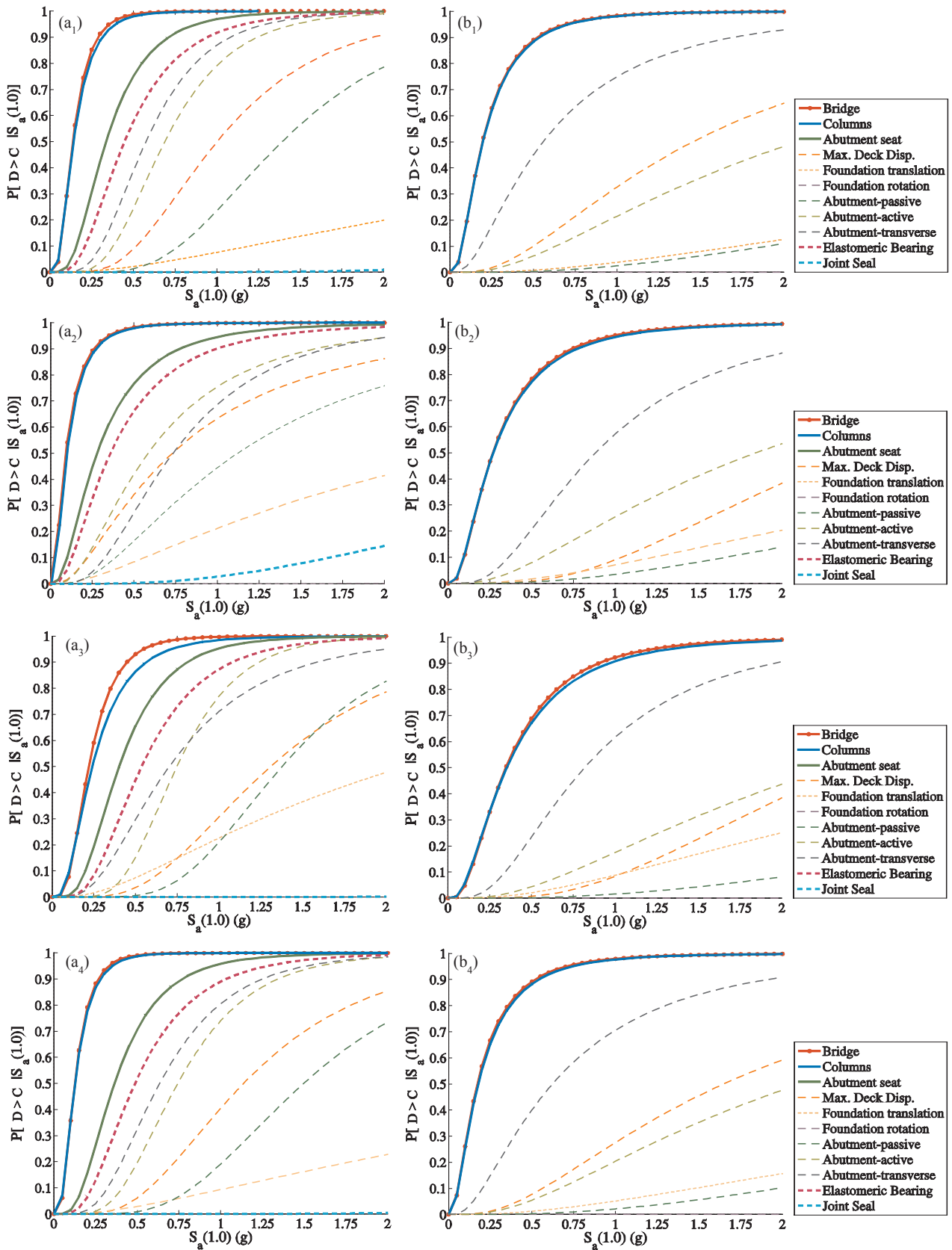


Fig. 17. Fragility curves at moderate damage state for the bridge system and components for bridges designed after 1970 with multi-columns per bent and (a) seat, (b) integral type abutment.

Table 7
Mean and standard deviation of system fragility curves.

Case	Column shape	Damage state							
		Slight		Moderate		Extensive		Collapse	
		Median (λ)	Dispersion (ξ)	Median (λ)	Dispersion (ξ)	Median (λ)	Dispersion (ξ)	Median (λ)	Dispersion (ξ)
DBSC	CP	0.120	0.89	0.205	0.96	0.324	1.08	1.040	1.11
DBSC	RP	0.146	1.03	0.251	1.09	0.394	1.20	1.253	1.22
DBSC	OP	0.172	0.98	0.399	1.02	0.642	1.15	2.090	1.23
DBSC	FI	0.110	0.91	0.177	0.96	0.282	1.09	0.932	1.14
SBSC	CP	0.084	0.58	0.153	0.66	0.217	0.81	0.545	0.83
SBSC	RP	0.072	0.60	0.107	0.68	0.153	0.83	0.409	0.86
SBSC	OP	0.107	0.60	0.261	0.65	0.404	0.85	1.043	0.88
SBSC	FI	0.084	0.59	0.142	0.67	0.204	0.82	0.533	0.85
DBMC	CP	0.122	0.73	0.178	0.77	0.249	0.86	0.566	0.89
DBMC	RP	0.152	0.74	0.243	0.84	0.342	0.94	0.832	0.96
DBMC	OP	0.164	0.69	0.322	0.76	0.458	0.87	1.114	0.90
DBMC	FI	0.120	0.73	0.165	0.77	0.231	0.86	0.528	0.88
SBMC	CP	0.074	0.51	0.135	0.57	0.183	0.68	0.390	0.70
SBMC	RP	0.064	0.59	0.102	0.65	0.138	0.76	0.309	0.77
SBMC	OP	0.085	0.56	0.211	0.60	0.302	0.76	0.672	0.78
SBMC	FI	0.069	0.55	0.115	0.60	0.154	0.70	0.326	0.72
DASC	CP	0.126	0.82	0.225	0.88	0.345	1.01	1.029	1.03
DASC	RP	0.148	0.98	0.271	1.06	0.426	1.18	1.362	1.21
DASC	OP	0.169	0.94	0.411	0.97	0.667	1.11	2.131	1.19
DASC	FI	0.117	0.87	0.191	0.91	0.295	1.03	0.897	1.06
SASC	CP	0.085	0.56	0.162	0.63	0.233	0.80	0.597	0.82
SASC	RP	0.073	0.56	0.117	0.66	0.164	0.80	0.445	0.85
SASC	OP	0.101	0.58	0.264	0.62	0.414	0.82	1.057	0.84
SASC	FI	0.084	0.56	0.146	0.64	0.208	0.80	0.534	0.83
DAMC	CP	0.118	0.83	0.195	0.86	0.269	0.93	0.593	0.95
DAMC	RP	0.154	0.71	0.267	0.80	0.374	0.91	0.885	0.93
DAMC	OP	0.161	0.69	0.347	0.75	0.499	0.88	1.211	0.89
DAMC	FI	0.116	0.83	0.175	0.86	0.240	0.93	0.533	0.95
SAMC	CP	0.068	0.52	0.137	0.58	0.188	0.69	0.406	0.71
SAMC	RP	0.061	0.78	0.110	0.81	0.154	0.93	0.325	0.94
SAMC	OP	0.083	0.50	0.220	0.56	0.324	0.73	0.711	0.75
SAMC	FI	0.067	0.53	0.124	0.59	0.169	0.68	0.355	0.69

Acknowledgements

The authors would like to thank the California Department of Transportation (Caltrans) for providing the bridge plans. The conclusions of the current paper do not necessarily show the views of the Caltrans.

References

- [1] Shinozuka M, Feng MQ, Lee J, Naganuma T. Statistical analysis of fragility curves. *J Eng Mech-ASCE* 2000;126:1224–31.
- [2] Gardoni P, Mosalam KM, der Kiureghian A. Probabilistic seismic demand models and fragility estimates for RC bridges. *J Earthq Eng* 2003;7:79–106.
- [3] Mackie KR, Stojadinović B. Fragility basis for California highway overpass bridge seismic decision making. Berkeley: Pacific Earthquake Engineering Research Center, College of Engineering, University of California; 2005.
- [4] Nielson BG. Analytical fragility curves for highway bridges in moderate seismic zones [Doctoral dissertation, Georgia Institute of Technology]; 2005.
- [5] Padgett JE, DesRoches R. Methodology for the development of analytical fragility curves for retrofitted bridges. *Earthq Eng Struct Dynam* 2008;37(8):1157–74.
- [6] Zhong J, Gardoni P, Rosowky D, Haukaas T. Probabilistic seismic demand models and fragility estimates for reinforced concrete bridges with two-column bents. *J Eng Mech* 2008;134:495–504.
- [7] Sullivan I. Analytical seismic fragility curves for skewed multi-span steel girder bridges [Doctoral dissertation, Clemson University]; 2010.
- [8] Ramanathan KN. Next generation seismic fragility curves for California bridges incorporating the evolution in seismic design philosophy. Georgia Institute of Technology; 2012.
- [9] Yang CSW, Werner SD, DesRoches R. Seismic fragility analysis of skewed bridges in the central southeastern United States. *Eng Struct* 2015;83:116–28.
- [10] Soleimani F, Vidakovic B, DesRoches R, Padgett J. Identification of the significant uncertain parameters in the seismic response of irregular bridges. *Eng Struct* 2017;141:356–72.
- [11] Tanaka H, Park R. Seismic design and behavior of reinforced concrete columns with interlocking spirals. *ACI Struct J* 1993;90(2):192–203.
- [12] Wu TL, Ou YC, Yen-Liang Yin S, Wang JC, Wang PH, Ngo SH. Behavior of oblong and rectangular bridge columns with conventional tie and multi-spiral transverse reinforcement under combined axial and flexural loads. *J Chin Inst Eng* 2013;36(8):980–93.
- [13] Ingham JM, Priestley MJN, Seible F. Seismic response of bridge knee joints having columns with interlocking spirals. *Bull N Z Natl Soc Earthq Eng* 1997;30(2):114–32.
- [14] Ou YC, Ngo SH, Yin SY, Wang JC, Wang PH. Shear behavior of oblong bridge columns with innovative seven-spiral transverse reinforcement. *ACI Struct J* 2014;111(6):1339.
- [15] Caltrans. Seismic Design Criteria, Version 1.4. California Department of Transportation; 2006.
- [16] Sanchez AV, Priestley MJN, Seible F. Seismic performance of flared bridge columns (No. SSRP-97/06). San Diego: University of California; 1997.
- [17] Nada HM, Sanders DH, Saiidi MS. Seismic performance of RC bridge frames with architectural-flared columns (No. CCEER 03–03). Center for Earthquake Engineering Research, University of Nevada; 2003.
- [18] Wehbe NI, Saiidi MS, Sanders DH. Effects of confinement and flares on the seismic performance of reinforced concrete bridge columns (No. RDT-01-004, CCEER-97-2); 1997.
- [19] Mazzoni S, McKenna F, Scott MH, Fenves GL. OpenSEES command language manual. Pacific Earthquake Engineering Research Center; 2006.
- [20] Soleimani F, McKay M, Yang CSW, Kurtis KE, DesRoches R, Kahn LF. Cyclic testing and assessment of columns containing recycled concrete debris. *ACI Struct J* 2016;113(5):1009.
- [21] Chang GA, Mander JB. Seismic energy based fatigue damage analysis of bridge columns: Part 1: evaluation of seismic capacity. Buffalo, NY: National Center for Earthquake Engineering Research; 1994.
- [22] Menegotto M. Method of analysis for cyclically loaded RC plane frames including changes in geometry and non-elastic behavior of elements under combined normal force and bending. In: Proc. IABSE symposium on resistance and ultimate deformability of structures acted on by well defined repeated loads; 1973. p. 15–22.
- [23] Filippou FC, Bertero VV, Popov EP. Effects of bond deterioration on hysteretic behavior of reinforced concrete joints. Washington, DC: National Science Foundation; 1983.
- [24] Zhao J, Sritharan S. Modeling of strain penetration effects in fiber-based analysis of reinforced concrete structures. *ACI Struct J* 2007;104(2):133.
- [25] Soleimani F. Fragility of California bridges-development of modification factors

- [Doctoral dissertation, Georgia Institute of Technology]; 2017.
- [26] Schoettler MJ, Restrepo JI, Guerrini G, Duck DE, Carrea F. A full-scale, single-column bridge bent tested by shake-table excitation. Center for Civil Engineering Earthquake Research, Department of Civil Engineering, University of Nevada; 2012.
- [27] Code of Practice for the Design of Concrete Structures (NZS 3101, Part 1:1982 and Commentary on the Design of Concrete Structures (NZS 3101, Part 2:1982). Wellington: Standards Association of New Zealand.
- [28] Flores LM. Performance of existing reinforced concrete columns under bidirectional shear and axial loading. Research Rep., Berkley, CA: Univ. of California; 2004.
- [29] Baker JW, Lin T, Shahi SK, Jayaram N. New ground motion selection procedures and selected motions for the PEER transportation research program. Peer Report 2011;2011:3.
- [30] HAZUS-MH. Multi-hazard loss estimation methodology: earthquake model. Washington (DC): Department of Homeland Security, FEMA; 2003.
- [31] Cornell CA, Jalayer F, Hamburger RO, Foutch DA. Probabilistic basis for 2000 SAC federal emergency management agency steel moment frame guidelines. *J Struct Eng* 2002;128(4):526–33.
- [32] Mangalathu Sivasubramanian Pillai S. Performance based grouping and fragility analysis of box-girder bridges in California [Doctoral dissertation, Georgia Institute of Technology]; 2017.